Supporting Information

Impact of Single Point Mutations on the Excitonic Structure and Dynamics in a Fenna-Matthews-Olson Complex

Anton Khmelnitskiy,[†] Tonu Reinot,[#] and Ryszard Jankowiak[†‡]*

[†]Department of Chemistry and [‡]Department of Physics, Kansas State University, Manhattan, KS, USA

*Corresponding Author: E-mail: ryszard@ksu.edu
[#]Permanent address: 13025 Morehead, Chapel Hill, North Carolina 27517, U.S.A.

FMO mutants and methodologies used. Site-directed mutations in the *fmoA* gene of *Chlorobaculum tepidum*, which encodes the FMO protein, were created as previously described.[1] All mutants were prepared by Dr. R. Saer in the laboratory of Dr. R. Blankenship at the Washington University at Saint Louis; for details see ref 1. Our experimental setup is also described elsewhere.[2] Here we only note that all low temperature absorption spectra were obtained with a spectral resolution of 4 cm^{-1}, while resonant HB spectra were obtained with 1-2 cm^{-1} spectral resolutions. Fluorescence spectra were collected, with a resolution of 0.1 nm, by a Princeton Instruments Acton SP-2300 spectrograph equipped with a back-illuminated CCD camera (PI Acton Spec10, 1340 × 400). The laser source (λ = 488.0 nm) for fluorescence and (nonresonant) HB spectra was produced by a Coherent Innova 90 argon ion laser. Laser power was set by a continuously adjustable neutral density filter. Holes excited within the 820-790 nm spectral range were obtained with Coherent CR-899 laser system. Experiments were performed at 4 K inside Oxford Instruments Optistat CF2 cryostat. Sample temperature was read and controlled with a Lakeshore Cryotronic model 330 or Mercury iTC temperature controller for the former and latter cryostats, respectively.

Details of our modeling approach are described in refs 3,4. In brief the disorder is introduced into the diagonal matrix elements (i.e., E_0^n) by a Monte-Carlo approach with normal distributions centered at E_0^n (*n* labeling various pigments, i.e., *n* = 1-24) and with *fwhm* representing Γ_{inh}, which can be site-dependent or independent. Eigen decomposition of the interaction matrix provides eigen-coefficients (c_n^M) and eigenvalues (ω_M). Phonon and vibrational Huang-Rhys (*S*) factors are used as free or fixed parameters and are optimized simultaneously against the experimental spectra. It is assumed that the phonon spectral density (weighted phonon profile) can be described by a continuous function, which is chosen to be a lognormal distribution, as illustrated in ref 5. We use experimentally determined phonon spectral density $J_{ph}(\omega)$[5,6] for BChl 3, a broader spectral density shape for the remaining pigments (for details see ref [7]), and vibrational spectral density $J_{vib}(\omega)$[6]. Intramolecular vibrational modes (J_{vib}) are considered to be dynamically localized[8]. S_{ph} = 0.4 while S_{vib} = 0.19 and 0.3 for absorption and emission spectra, respectively. In simulations of optical spectra we use non-Markovian density matrix (Redfield theory) with Monte Carlo disorder averaging and Nelder-Mead Simplex algorithm for parameter optimization.[9] Our in-house written software can simultaneously fit

several experimental spectra at different temperatures, providing constraints on the pigment site energies of interest.

On inter-monomer uncorrelated (incoherent) EET. The general consensus is that ps and sub-ps excitation energy transfer (EET) takes place in each monomer of the FMO trimer, while inter-monomer uncorrelated EET times are much slower; (see Table S1 below).[10,11] Inter-domain energy transfer is assumed to proceed via incoherent hopping described by the Generalized Förster equation.[12] In practice, for generalized Förster theory domains are determined by setting certain off-diagonal elements of the Hamiltonian to zero, thus restricting the extent of exciton delocalization. In a simple approximation we assume all couplings smaller than reorganization energy should be zeroed. To properly describe emission and nonresonant HB spectra one needs to consider the uncorrelated (incoherent) EET between the three monomers of the WT FMO trimer. Due to disorder and EET between BChl 3 pigments (and in part BChl 4 molecules, which have small probability to be the lowest energy pigments) in the three FMO monomers, the lowest energy absorption band near 825 nm is contributed by three sub-bands (i.e. the three excitonic states of the trimer as demonstrated in Figure S1. Table S1 shows the calculated Förster energy transfer times in ps between the three lowest-energy excitonic states (columns) of the trimer for WT, V152N, S73A and W184F FMO mutants, respectively.

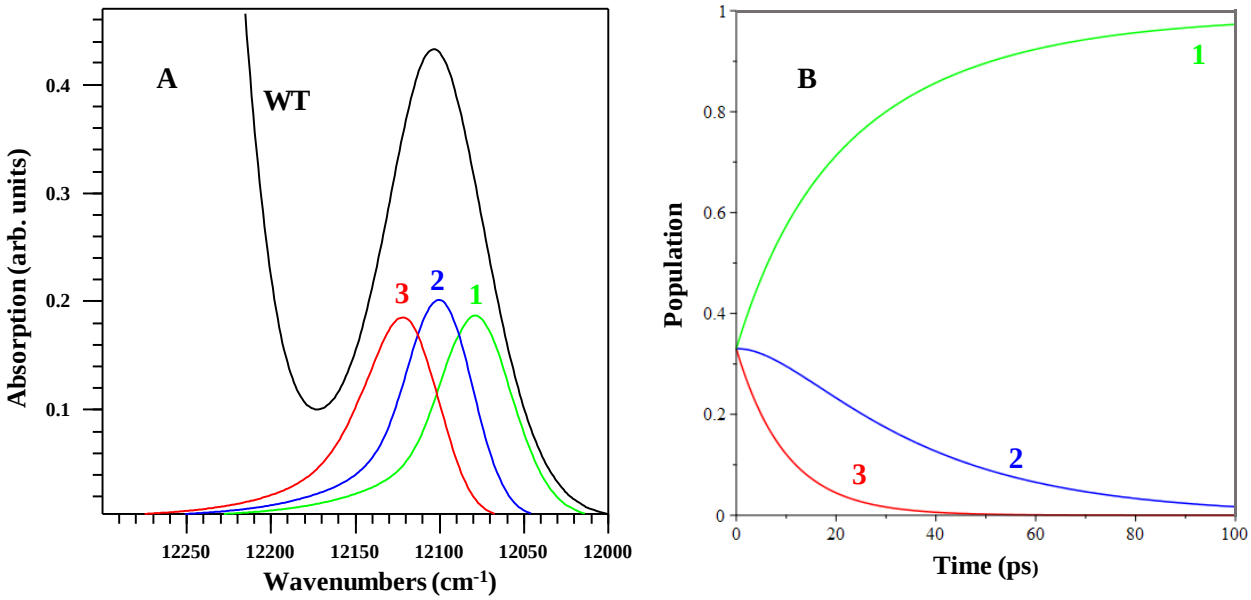

Figure S1. *Frame A*: Lowest-energy band of WT FMO absorption at 4 K (black) and calculated three lowest-energy excitonic states with phonons (labeled as 1, 2 and 3). For perfect EET to the lowest energy fraction of FMO complexes, long-lived emission originates only from sub-state 1. Also, only these pigments are bleached as revealed by fitting of the nonresonant HB spectrum (see main text). *Frame B*: Simulated excitation Förster dynamics at 4 K between three domains of FMO trimer assuming equal initial population of lowest exciton states in each domain as a result of fast intradomain energy relaxation.

Table S1. Calculated Förster energy transfer times in ps between the three lowest-energy excitonic states (columns) of the trimer for WT, V152N, S73A and W184F FMO mutants respectively. Labeling of bands 1,2, and 3 is shown in Figure S1.

	WT	**V152N**	**S73A**	**W184F**
3→2	17	15	13	12
2→1	16	14	10	11
3→1	47	35	25	20

***Calculation of nonresonant HB spectra*.** In order to calculate HB spectra one must assign a new site energy to pigment *m* after the HB process. The simplest approximation, used in refs 13,14, is to assume that after the HB transition, the protein can end up in any of the conformational sub-states that are present in the original inhomogeneous ensemble around a particular chromophore. This assumption worked well while modeling nonresonant HB spectra obtained for CP29[15] and WSCP.[14] However, the average distribution of particular pigment contributing to the lowest-energy exciton (only the lowest exciton state is populated in an excitonically coupled system like FMO) may also change. That is, due to protein conformational flexibility and complexity of its energy landscape, it is possible that during the HB process conformational transitions occur shifting the average post-burn site-energy distribution of a particular BChl contributing to the lowest-energy exciton. This is the case in WT_I where, to properly describe the nonresonant hole, the site-energies of BChls 3 and 4 had to be shifted by 36 and 252 cm^{-1}, respectively.[4] For description of HB spectra of various mutants see the main text.

Table S2. Hole widths (Γ_{ZPH}), hole depths and corresponding effective excited-state decay times (T_1) as a function of burn frequency (ν_B) obtained for various FMO samples burned with a constant fluence of 6 J/cm^2 (V152N, W184F, S73A) or 12 J/cm^2 (for a typical WT FMO).

Sample	**Wavenumber**	**Hole depth (%)**	**Resolution corrected Γ_{ZPH} (cm^{-1})**	**T_1 (ps)**
V152N	12283	2.8	6.4	1.7
	12312	3.6	6.4	1.7
	12343	5.6	5.3	2.0
	12403	2.3	8.5	1.2
	12436	1.4	10.0	1.1
	12468	1.4	10.6	1.0
	12500	1.8	11.0	1.0
	12530	1.9	10.6	1.0
	12561	1.8	10.6	1.0
	12593	1.5	8.5	1.0
W184F	12282	3.3	6.4	1.7
	12313	4.0	6.4	1.7
	12343	4.1	7.5	1.4
	12374	4.2	7.5	1.4
	12404	3.0	7.5	1.4
	12436	2.5	7.5	1.4

	12468	2.4	6.9	1.5
	12499	1.9	7.5	1.4
	12530	1.8	6.9	1.5
	12561	1.5	9.0	1.2
	12593	1.3	5.5	1.9
S73A	12404	2.0	7.5	1.4
	12373	5.0	5.3	1.7
	12342	7.0	4.7	2.3
	12313	5.0	6.4	2.0
	12282	3.0	7.5	1.4
typical WT FMO	12342	5.0	6.6	1.6
	12373	3.2	7.8	1.4
	12407	1.1	9.6	1.1

Mutant V152N. We showed recently that to properly fit absorption, fluorescence, nonresonant hole-burned (NRHB) and circular dichroism (CD) spectra at low temperature BChl 8 of each subunit should be placed in separate domain from 7 other pigments.[4] Thus, excitonic states (no phonons and vibrations were included) of the monomer of WT and mutant FMO were calculated without BChl 8 whose contribution was calculated separately and added to a graph later. Figure S2 illustrates seven excitonic states of the monomer of V152N mutant plus contribution to the calculated absorption by BChl 8, while Figure S3 shows BChls 1-8 contributions ($d_m(\omega)$) to the calculated absorption spectrum of V152N mutant shown in Figure 3 in the main text.

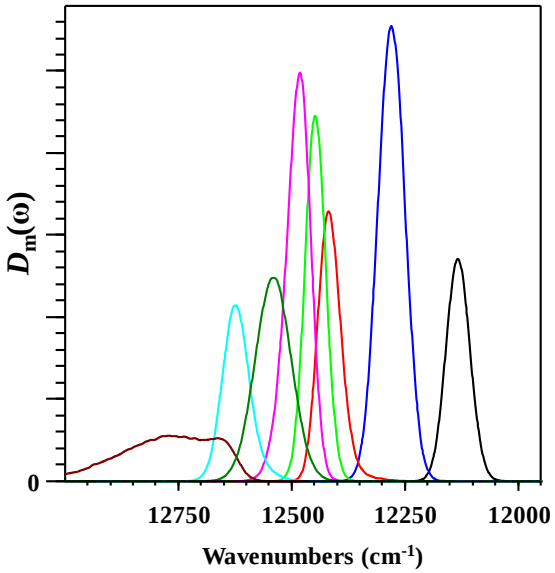

Figure S2. Seven excitonic states of the monomer of V152N mutant plus contribution to the calculated absorption by BChl 8 (dark green curve; i.e. third from the left).

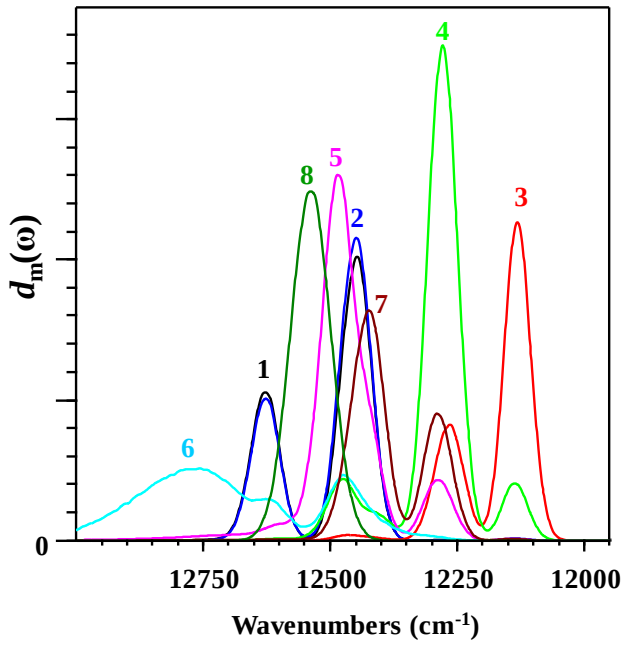

Figure S3. BChls 1-8 contributions ($d_m(\omega)$) to the calculated absorption spectrum of V152N mutant shown in Figure 3 in the main manuscript.

Table S3 shows the contribution numbers ($|c_{mM}|^2$) of pigments *m* to monomeric excitonic states *M* obtained from simultaneous fits of absorption, emission, and nonresonant HB spectra shown in Figure 3 of the main manuscript. Delocalization lengths (L_M) are shown at the bottom of table S3. Frenkel exciton Hamiltonian for the V152N mutant FMO trimer in the site representation is shown in table S4.

Table S3. Contribution numbers ($|c_{mM}|^2$) of pigments *m* to monomeric excitonic states *M* and delocalization lengths (L_M) found from simultaneous fits of spectra shown in Figure 3 (main paper) obtained for V152N mutant.

	M						
m	**1**	**2**	**3**	**4**	**5**	**6**	**7**
1	0	0	0.11	0.27	0.11	0.4	0.11
2	0.01	0	0.1	0.27	0.14	0.38	0.1
3	0.84	0.15	0.01	0	0.01	0	0
4	0.15	0.62	0.08	0.05	0.09	0.01	0
5	0	0.08	0.14	0.17	0.49	0.08	0.05
6	0	0.01	0.03	0.04	0.08	0.12	0.72
7	0.01	0.15	0.53	0.21	0.09	0.01	0.01
L_M	1.39	2.16	1.85	2.27	2.13	2.16	1.53

Table S4. Frenkel exciton Hamiltonian for the V152N mutant FMO trimer in the site representation. Pigment site energies/inhomogeneous broadening (*fwhm*; in blue) are on the diagonal. Off-diagonal numbers are coupling matrix elements (V_{nm}).

BChl *a*	**1**	**2**	**3**	**4**	**5**	**6**	**7**	**8**[#]
1	12530/110	-87	4.2	-5.2	5.5	-14	-6.1	0
2		12555/110	28	6.9	1.5	8.7	4.5	0
3			12155/70	-54	-0.2	-7.6	1.2	0
4				12304/113	-62	-16	-51	0
5					12475/110	60	1.7	0
6						12690/320	29	0
7							12400/110	0
8[#]								12515/110

Mutant W184F. Figure S4 illustrates seven excitonic states of the monomer of W184F mutant plus contribution to the calculated absorption by BChl 8, while Figure S5 shows BChls 1-8 contributions ($d_m(\omega)$) to the calculated absorption spectrum of W184F mutant shown in Figure 4C in the main text. Frenkel exciton Hamiltonian for the W184F mutant FMO trimer in the site representation is shown in Table S5. Table S6 shows the contribution numbers ($|c_{mM}|^2$) of pigments *m* to monomeric excitonic states *M* obtained from simultaneous fits of absorption, emission, and nonresonant HB spectra shown in Figure 4C of the main manuscript. Delocalization lengths (L_M) are shown at the bottom of Table S6.

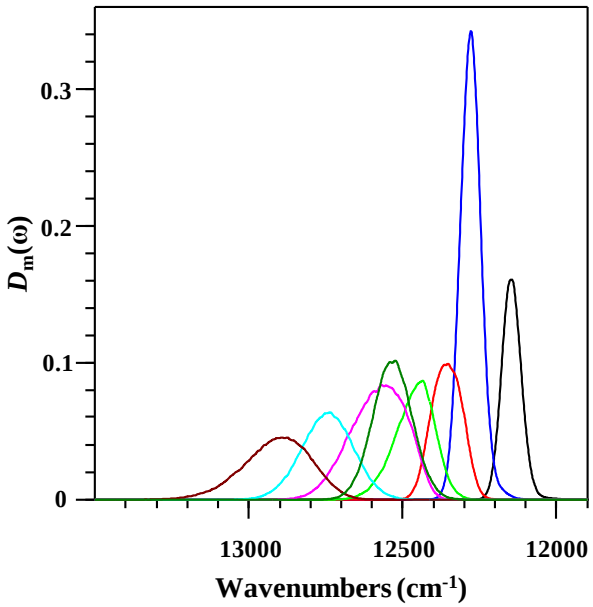

Figure S4. Seven excitonic states of the monomer of W184F FMO mutant plus contribution to the calculated absorption by BChl 8 (dark green curve; i.e. 4th curve from the left).

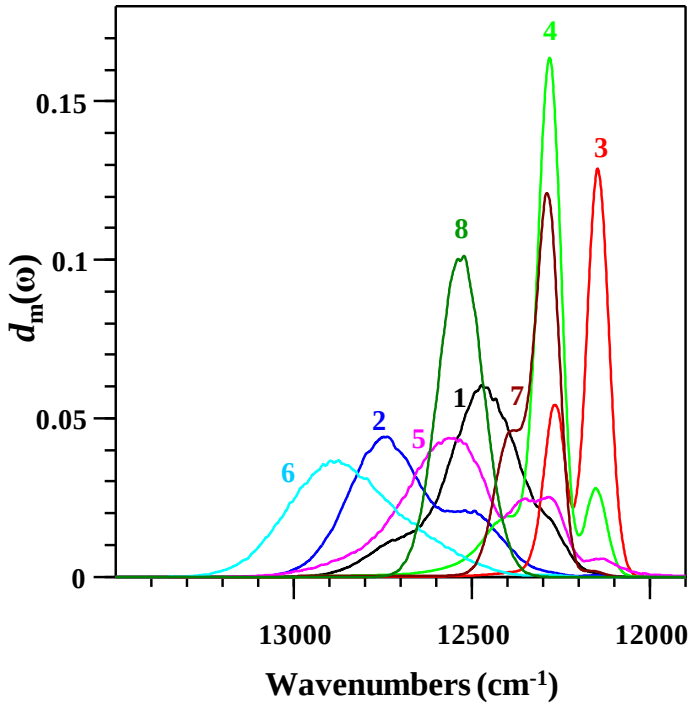

Figure S5. BChls 1-8 contributions ($d_m(\omega)$) to the calculated absorption spectrum of W184F FMO mutant shown in Figure 4.

Table S5. Frenkel exciton Hamiltonian for the W184F FMO trimer in the site representation. Pigment site energies/inhomogeneous broadening (*fwhm*; in blue) are on the diagonal. Off-diagonal numbers are coupling matrix elements (V_{nm}).

BChl *a*	**1**	**2**	**3**	**4**	**5**	**6**	**7**	**8**[#]
1	12499/270	-87	4.2	-5.2	5.5	-14	-6.1	0
2		12697/270	28	6.9	1.5	8.7	4.5	0
3			12174/83	-54	-0.2	-7.6	1.2	0
4				12315/124	-62	-16	-51	0
5					12528/415	60	1.7	0
6						12852/320	29	0
7							12363/107	0
8								12532/149

Table S6. Contribution numbers ($|c_{mM}|^2$) of pigments *m* to monomeric excitonic states *M* for mutant W184F and corresponding delocalization lengths (L_M).

	M						
m	**1**	**2**	**3**	**4**	**5**	**6**	**7**

1	0.00	0.04	0.17	0.37	0.24	0.15	0.03
2	0.00	0.00	0.02	0.10	0.16	0.54	0.17
3	0.79	0.17	0.03	0.01	0.00	0.00	0.00
4	0.16	0.41	0.21	0.14	0.07	0.01	0.00
5	0.04	0.11	0.11	0.15	0.41	0.11	0.08
6	0.00	0.00	0.00	0.02	0.08	0.19	0.71
7	0.01	0.27	0.45	0.22	0.04	0.00	0.00
L_M	1.47	2.28	1.94	1.83	1.71	1.55	1.30

Mutant S73A. Due to pheophytinization of BChl 2 in 2/3 of the FMO complexes, excitonic states, pigment contributions to absorption and pigment contributions to excitonic states were calculated separately for pheophytinized and non-pheophytinized subunits. Figure S6A and S6B show seven excitonic states of the monomer containing BPheo 2 (Frame A) or BChl 2 (Frame B), respectively. The dark green curve shows by BChl 8 contribution to the calculated absorption spectrum. Pigment 1-8 contributions ($d_m(\omega)$) to the calculated absorption spectrum for the monomer of S73A mutant containing BPheo 2 (Frame A) or BChl 2 (Frame B) are shown in Figure S7 (frames A and B, respectively).

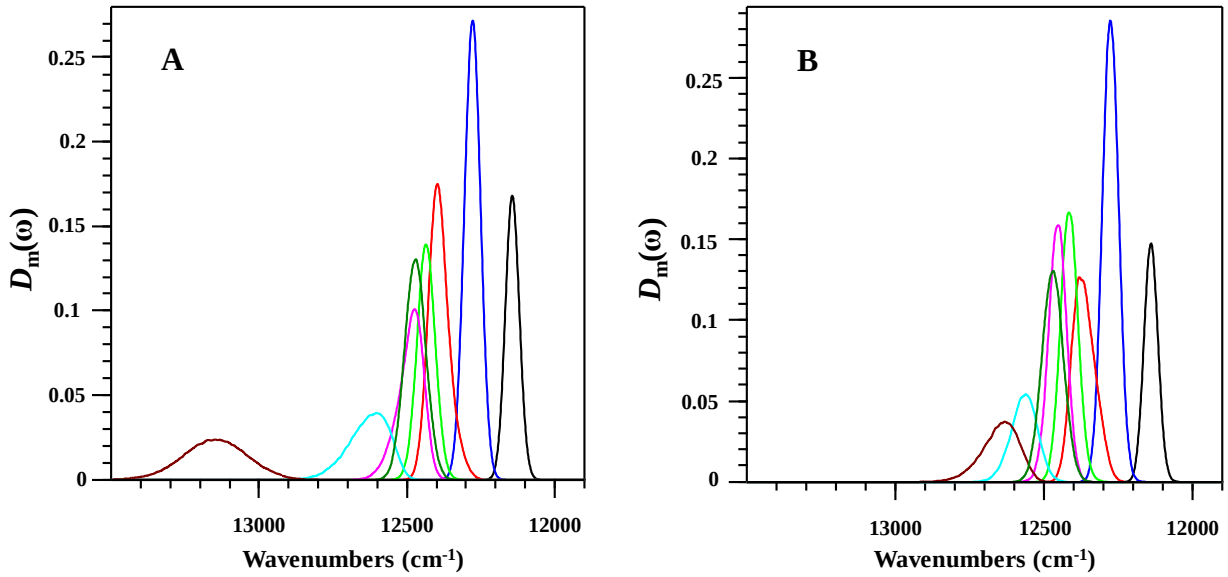

Figure S6. Seven excitonic states of the monomer of S73A containing BPheo 2 (Frame A) or BChl 2 (Frame B), respectively.

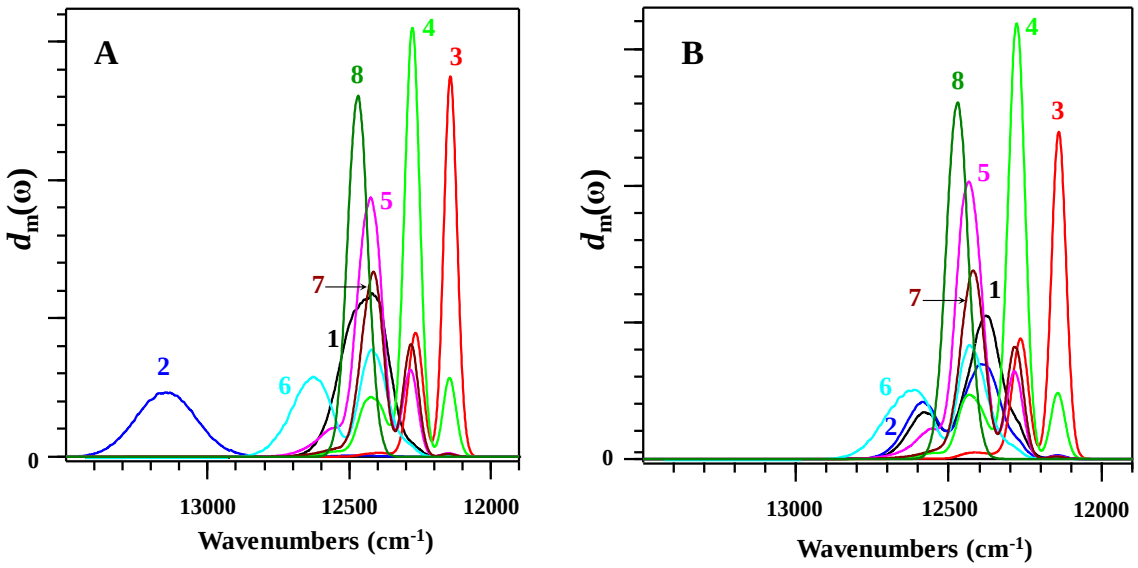

Figure S7. Pigment 1-8 contributions ($d_m(\omega)$) to the calculated absorption spectrum for the FMO monomer of S73A mutant containing BPheo 2 (Frame A) or BChl 2 (Frame B).

Calculated pigment contributions to various excitonic states of the monomer of S73A mutant containing BPheo 2 or BChl 2 are demonstrated in Tables S7 and S8, respectively. Frenkel exciton Hamiltonian for the S73A mutant FMO trimer in the site representation is shown in Table S9.

Table S7. Contribution numbers ($|c_{mM}|^2$) of pigments *m* to excitonic states *M* of the FMO monomer of S73A mutant containing BPheo 2 and delocalization lengths (L_M).

	M						
m	**1**	**2**	**3**	**4**	**5**	**6**	**7**
1	0.00	0.02	0.25	0.21	0.45	0.06	0.01
2	0.00	0.00	0.00	0.00	0.00	0.00	0.99
3	0.82	0.16	0.01	0.01	0.00	0.00	0.00
4	0.17	0.55	0.09	0.09	0.06	0.04	0.00
5	0.01	0.12	0.23	0.24	0.22	0.19	0.00
6	0.00	0.02	0.11	0.11	0.10	0.66	0.00
7	0.01	0.14	0.30	0.34	0.16	0.05	0.00
L_M	2.41	2.19	1.98	1.88	1.79	1.43	1.02

Table S8. Contribution numbers ($|c_{mM}|^2$) of pigments *m* to excitonic states *M* of the FMO monomer of S73A mutant containing BChl 2 and delocalization lengths (L_M).

	M						
m	**1**	**2**	**3**	**4**	**5**	**6**	**7**
1	0.00	0.04	0.34	0.13	0.08	0.25	0.16

2	0.01	0.03	0.23	0.10	0.08	0.32	0.24
3	0.82	0.14	0.02	0.01	0.01	0.00	0.00
4	0.16	0.53	0.08	0.08	0.10	0.03	0.01
5	0.01	0.11	0.12	0.23	0.29	0.15	0.09
6	0.00	0.01	0.06	0.10	0.14	0.21	0.47
7	0.01	0.13	0.15	0.35	0.30	0.04	0.03
L_M	1.44	2.42	2.14	2.27	2.34	2.33	1.91

Table S9. Frenkel exciton Hamiltonian for the S73A mutant FMO trimer in the site representation. Pigment site energies/inhomogeneous broadening (*fwhm*; in blue) are on the diagonal. Off-diagonal numbers are coupling matrix elements (V_{nm}).

BChl *a*	1	2	3	4	5	6	7	8[#]
1	12460/175	-87	4.2	-5.2	5.5	-14	-6.1	0
2		12495/185 (13140/250)*	28	6.9	1.5	8.7	4.5	0
3			12166/63	-54	-0.2	-7.6	1.2	0
4				12300/100	-62	-16	-51	0
5					12444/100	60	1.7	0
6						12560/225	29	0
7							12410/110	0
8[#]								12470/84

*BPheo 2

Modeling of optical spectra obtained for Y345F, F243Y and Q198V mutants.

Experimental and calculated absorption, fluorescence, and NRHB spectra for FMO mutants Y345F (mutation near BChl 4), F243Y (mutation near BChl 5) and Q198V (mutation near BChl 7) are provided in Figures S8-S10, respectively.

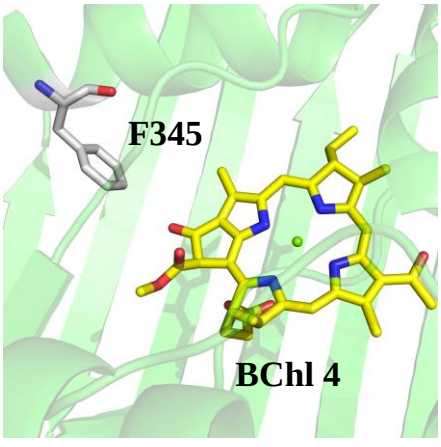

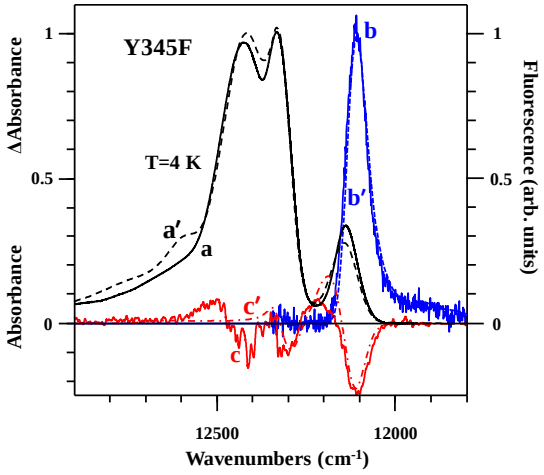

Figure S8. Left frame: Y345F mutant. Right frame: Experimental (solid) and calculated (dashed) absorbance (black curves a/a′), experimental (solid) emission and calculated (dotted) emission (blue curves b/b′), experimental (solid) and calculated (dashed-dotted) HB spectra (ν_{ex}/ν_B = 12407 cm^{-1}) (red curves c/c′) curves for Y345F FMO mutant.

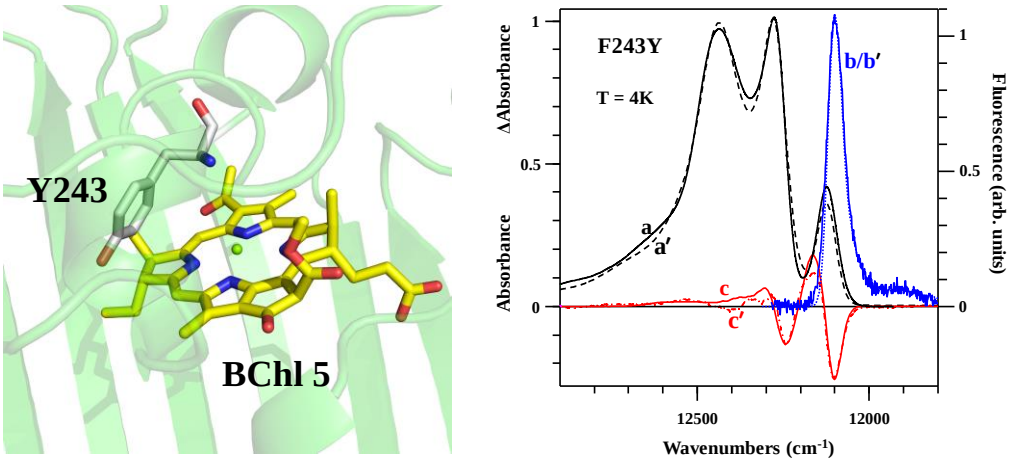

Figure S9. Left frame: F243Y mutant. Right frame: Experimental (solid) and calculated (dashed) absorbance (black curves a/a′), experimental (solid) emission and calculated (dotted) emission (blue curves b/b′), experimental (solid) and calculated (dashed-dotted) HB spectra (ν_{ex}/ν_B = 20490 cm^{-1}) (red curves c/c′) curves for F243Y FMO mutant.

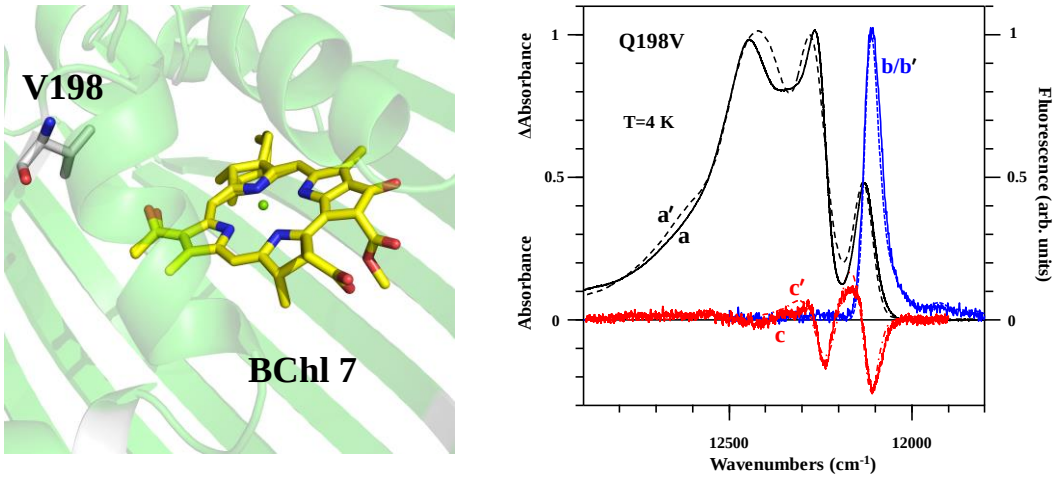

Figure S10. Left frame: Q198V mutant. Right frame: Experimental (solid) and calculated (dashed) absorbance (black curves a/a′), experimental (solid) emission and calculated (dotted) emission (blue curves b/b′), experimental (solid) and calculated (dashed-dotted) HB spectra (ν_{ex}/ν_B = 20490 cm^{-1}) (red curves c/c′) curves for Q198V FMO mutant.

Absorption (black) and hole-burned spectra (red) at λ_B = 800 – 802 nm obtained for Y345F, F243Y, and Q198V mutants are shown in Figures S11-S13, respectively.

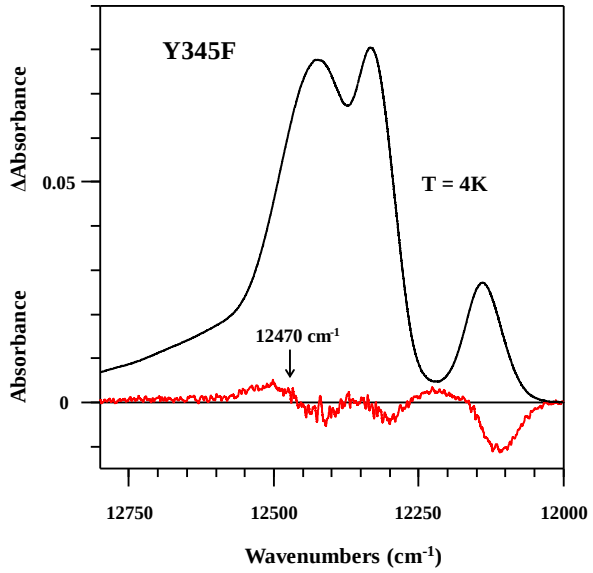

Figure S11. Y345F mutant absorption (black) and hole-burned spectrum obtained under excitation at 12470 cm^{-1} (802 nm) with fluence of 6 J/cm^2.

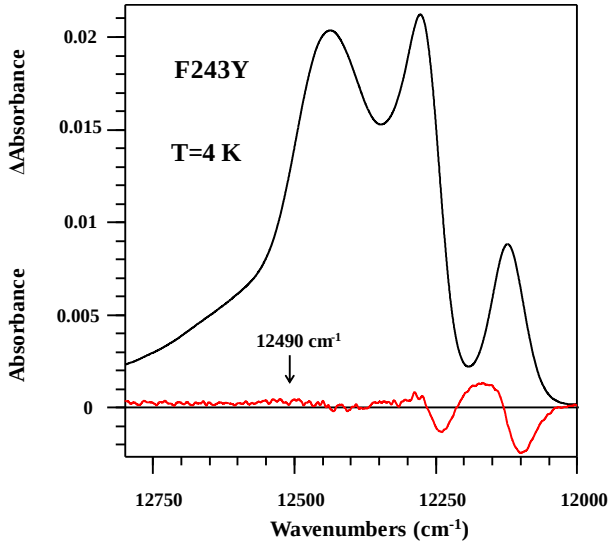

Figure S12. F243Y mutant absorption (black) and hole-burned spectrum obtained under excitation at 12490 cm^{-1} (800.6 nm) with fluence of 12 J/cm^2.

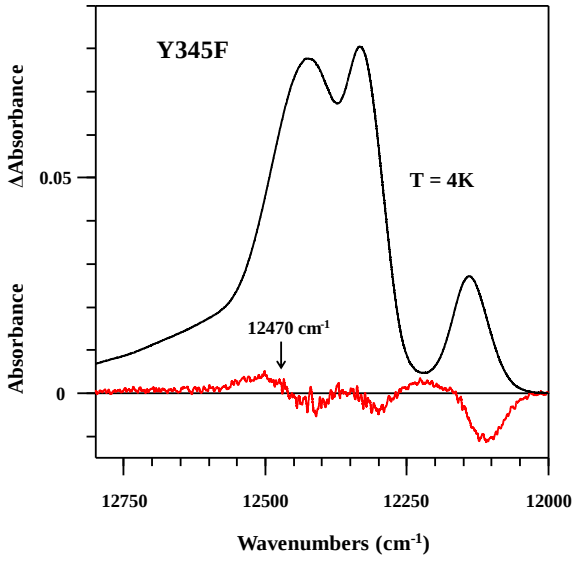

Figure S13. Q198V mutant absorption (black) and hole-burned spectrum obtained under excitation at 12470 cm^{-1} (802 nm) with fluence of 6 J/cm^2.

Finally, Table S10 summarizes site energy shifts calculated for various FMO mutants, studied in our laboratory, in comparison to WT sample. Comparison of calculated energy shifts among the mutants for pigments not directly affected by single point mutations (with possible exception of highly heterogeneous mutant Y16F)[16] may help to estimate accuracy of pigment site energy assignments. For example, it is well established that BChl 3 has the lowest site energy and is a main contributor to distinct lowest energy absorption band at ~825 nm which facilitate accurate site energy assignment for that pigment.[7,11,17,18] Unsurprisingly, site energy of BChl 3 varies little from mutant to mutant (except mutant Y16F, see Table S10), undergoing the largest shift of 25 cm^{-1} to higher energy in Q198V mutant. Bearing in mind that this band can blue-shift up to ~20 cm^{-1} in some samples due to possible destabilization during isolation procedure,[4,19] site energy assignment for BChl 3 should be considered accurate. Similar or even higher accuracy is likely achieved for BChl 4 which is a second major contributor to the band at ~825 nm and a major contributor to the band at ~815 nm. As can be seen from the Table S8, the site energy spread for six other pigments is obviously higher in all mutants and indirect influence of some mutations on their site energies cannot be discarded. The drastic example is Y16F mutant (see ref 16) which should be excluded from comparison accordingly. Caution should be taken also for mutant W184F, as its emission has a weak blue-shifted contribution indicating to some, albeit not large, heterogeneity. Nevertheless, site energy variations for the pigments in all other mutants from Table S10 are still smaller than *fwhm* of respective SDFs and therefore their site energies can be considered reasonably accurate.

Table S10. Difference between pigment site energies of WT and corresponding mutant.

BChl a	V152N	S73A	Y16F(Sub_{821})	Y16F(Sub_{817})	Y345F	F243Y	W184F	Q198V
1	**80**	-3	-22	-22	0	-35	37	-52
2	48	**654(9)***	-72	-72	40	-43	211	88
3	5	15	**101**	**168**	25	10	23	25
4	-18	-16	208	180	**65**	1	-1	-12
5	18	-14	67	67	2	**8**	70	49
6	98	-53	120	120	97	-14	**238**	51
7	39	43	48	48	88	69	-5	**26**
8	40	10	0	0	-42	-9	72	-12

---

*For BPheo(BChl)

References

(1) Saer, R.; Orf, G. S.; Lu, X.; Zhang, H.; Cuneo, M. J.; Myles, D. A. A.; Blankenship, R. E. Perturbation of Bacteriochlorophyll Molecules in Fenna-Matthews-Olson Protein Complexes through Mutagenesis of Cysteine Residues. *Biochim. Biophys. Acta - Bioenerg.* **2016**, *1857*, 1455–1463.

(2) Feng, X.; Neupane, B.; Acharya, K.; Zazubovich, V.; Picorel, R.; Seibert, M.; Jankowiak, R. Spectroscopic Study of the CP43′ Complex and the PSI–CP43′ Supercomplex of the Cyanobacterium Synechocystis PCC 6803. *J. Phys. Chem. B* **2011**, *115*, 13339–13349.

(3) Kell, A.; Blankenship, R. E.; Jankowiak, R. Effect of Spectral Density Shapes on the Excitonic Structure and Dynamics of the Fenna–Matthews–Olson Trimer from Chlorobaculum Tepidum. *J. Phys. Chem. A* **2016**, *120*, 6146–6154.

(4) Khmelnitskiy, A.; Kell, A.; Reinot, T.; Saer, R. G.; Blankenship, R. E.; Jankowiak, R. Energy Landscape of the Intact and Destabilized FMO Antennas from C. Tepidum and the L122Q Mutant: Low Temperature Spectroscopy and Modeling Study. *Biochim. Biophys. Acta - Bioenerg.* **2018**, *1859*, 165–173.

(5) Kell, A.; Feng, X.; Reppert, M.; Jankowiak, R. On the Shape of the Phonon Spectral Density in Photosynthetic Complexes. *J. Phys. Chem. B* **2013**, *117*, 7317–7323.

(6) Rätsep, M.; Freiberg, A. Electron-Phonon and Vibronic Couplings in the FMO Bacteriochlorophyll a Antenna Complex Studied by Difference Fluorescence Line Narrowing. *J. Lumin.* **2007**, *127*, 251–259.

(7) Kell, A.; Blankenship, R. E.; Jankowiak, R. Effect of Spectral Density Shapes on the Excitonic Structure and Dynamics of the Fenna–Matthews–Olson Trimer from Chlorobaculum Tepidum. *J. Phys. Chem. A* **2016**, *120*, 6146–6154.

(8) Renger, T.; Madjet, M. E.; Knorr, A.; Müh, F. How the Molecular Structure Determines the Flow of Excitation Energy in Plant Light-Harvesting Complex II. *J. Plant Physiol.* **2011**, *168*, 1497–1509.

(9) Nelder, J. A.; Mead, R. A Simplex Method for Function Minimization. *Comput. J.* **1965**, *7*, 308–313.

(10) Thyrhaug, E.; Žídek, K.; Dostál, J.; Bína, D.; Zigmantas, D. Exciton Structure and Energy Transfer in the Fenna–Matthews–Olson Complex. *J. Phys. Chem. Lett.* **2016**, *7*, 1653–1660.

(11) Cho, M.; Vaswani, H. M.; Brixner, T.; Stenger, J.; Fleming, G. R. Exciton Analysis in 2D Electronic Spectroscopy. *J. Phys. Chem. B* **2005**, *109*, 10542–10556.

(12) Raszewski, G.; Renger, T. Light Harvesting in Photosystem II Core Complexes Is Limited by the Transfer to the Trap: Can the Core Complex Turn into a Photoprotective Mode? *J. Am. Chem. Soc.* **2008**, *130*, 4431–4446.

(13) Reppert, M. Modeling of Resonant Hole-Burning Spectra in Excitonically Coupled Systems: The Effects of Energy-Transfer Broadening. *J. Phys. Chem. Lett.* **2011**, *2*, 2716–2721.

(14) Adolphs, J.; Berrer, M.; Renger, T. Hole-Burning Spectroscopy on Excitonically Coupled Pigments in Proteins: Theory Meets Experiment. *J. Am. Chem. Soc.* **2016**, *138*, 2993–3001.

(15) Feng, X.; Pan, X.; Li, M.; Pieper, J.; Chang, W.; Jankowiak, R. Spectroscopic Study of the Light-Harvesting CP29 Antenna Complex of Photosystem II—Part I. *J. Phys. Chem. B* **2013**, *117*, 6585–6592.

(16) Khmelnitskiy, A.; Saer, R. G.; Blankenship, R. E.; Jankowiak, R. Excitonic Energy Landscape of the Y16F Mutant of the Chlorobium Tepidum Fenna–Matthews–Olson (FMO) Complex: High Resolution Spectroscopic and Modeling Studies. *J. Phys. Chem. B* **2018**, *122*, 3734–3743.

(17) Adolphs, J.; Renger, T. How Proteins Trigger Excitation Energy Transfer in the FMO Complex of Green Sulfur Bacteria. *Biophys. J.* **2006**, *91*, 2778–2797.

(18) Vulto, S. I. E.; de Baat, M. A.; Louwe, R. J. W.; Permentier, H. P.; Neef, T.; Miller, M.; van Amerongen, H.; Aartsma, T. J. Exciton Simulations of Optical Spectra of the FMO Complex from the Green Sulfur Bacterium Chlorobium Tepidum at 6 K. *J. Phys. Chem. B* **1998**, *102*, 9577–9582.

(19) Kell, A.; Acharya, K.; Blankenship, R. E.; Jankowiak, R. On Destabilization of the Fenna-Matthews-Olson Complex of Chlorobaculum Tepidum. *Photosynth. Res.* **2014**, *120*, 323–329.